Urban Climate 33 (2020) 100648

Contents lists available at ScienceDirect

Urban Climate

journal homepage: www.elsevier.com/locate/uclim

A novel method to improve temperature forecast in data-scarce urban environments with application to the Urban Heat Island in Beirut

Mohamad Ghadban[a], Abdelkader Baayoun[a], Issam Lakkis[a,*], Sara Najem[b], Najat A. Saliba[c], Alan Shihadeh[a]

[a] Department of Mechanical Engineering, American University of Beirut, Beirut 1107 2020, Lebanon
[b] National Center for Remote Sensing, National Council for Scientific Research (CNRS), Riad al Soloh, 1107 2260, Beirut, Lebanon
[c] Department of Chemistry, American University of Beirut, Beirut 1107 2020, Lebanon

ARTICLE INFO

Keywords:
WRF
Urban canopy model
Anthropogenic heat
Albedo
Urban heat island

ABSTRACT

The urban heat island (UHI) effect has been the subject of much research due to its adverse effects on health, energy, and the environment. The objective of this work is to investigate the key parameters contributing to the urban heat island effect in Beirut city and to improve the temperature forecast in the city by taking these parameters into account. This is accomplished by coupling the single – layer urban canopy model (UCM) with the Weather Research and Forecasting model (WRF), where the urban parameters in UCM are calculated or fine – tuned to minimize the difference between the measured and the forecasted temperature. Urban parameters that were tuned included the roof albedo, wall albedo, roof thermal conductivity, in addition to the anthropogenic heat. To get optimum values for these parameters, simulations with different values for each parameter were performed during the four seasons and compared with observations from stations that are distributed across the city using a novel method that has not been used before to the best of our knowledge. Comparison is based on the mean, standard deviation, mean bias, root mean square error, and correlation coefficient. We also present an assessment of the UHI in Beirut based on some metrics of urban complexity.

1. Introduction

Beirut, the capital of Lebanon, is a coastal city that lies on the eastern shore of the Mediterranean Sea. Beirut city (administrative area) spans an area of about 18 km^2 and sits atop of two hills, Al-Achrafieh (East Beirut) and Al-Msaitbeh (West Beirut) (Beirut [Online], n.d.).

The city has witnessed rapid urbanization during the past thirty years. One of the main causes of this phenomenon was the civil war which started in 1975 and led to a catastrophic destruction of many buildings in Beirut. Consequently, a massive construction movement started after the war ended in 1990. Another reason for the rapid urban expansion in Beirut is the fact that economic levels in Beirut in terms of availability of jobs and salaries are generally better than those in other regions in Lebanon. Therefore, people from rural areas tend to move to Beirut for the sake of having a better living. As a matter of fact, according to the United Nations Human Settlements Programme (UN-Habitat) (UN-Habitat (2014, 2017)), 88% of Lebanon's population lived in urban areas in 2014.

* Corresponding author at: Department of Mechanical Engineering, American University of Beirut, Beirut 1107 2020, Lebanon.
E-mail address: issam.lakkis@aub.edu.lb (I. Lakkis).

https://doi.org/10.1016/j.uclim.2020.100648
Received 11 June 2019; Received in revised form 28 March 2020; Accepted 21 May 2020

With the need for proper accommodation, the previous figure clearly reflects the general urban status in Lebanon, particularly in Beirut. In addition, urban populations in Lebanon increased further due to the influx of refugees from conflict zones in neighboring countries. Based on the most recent data from the United Nations High Commissioner for Refugees (UNHCR) (UNHCR. (2/2/2019), n.d.) and ReliefWeb (ReliefWeb. (2/9/2019), n.d.), the influx of Syrian refugees resulted in 22% and 5% increase in the population of Lebanon and administrative Beirut, respectively. The increase in energy demand associated with this rapidly increasing urban population and the inability of the Lebanese government to meet this increase has led to the sprouting of diesel generators to fill the supply-demand gap (AEMS, 2017).

Notwithstanding its contribution to the urban economy (Liang and Yang, 2019), urbanization has a negative impact on the human health and the environment (Alberti, 2005; Lu, 2019). A key phenomenon is the urban heat island (UHI) effect which characterizes urban areas that are significantly warmer than their rural surroundings (Oke, 1967). The energy consumption to meet the demands of transportation, space heating, cooling, and domestic hot water use, is a major contributor to the UHI due to the anthropogenic heat release associated with the combustion of fossil fuel. Other aspects influencing the UHI include man-made structures and surfaces that affect the thermal dynamics and solar radiation interaction between the urban environment and the atmosphere. Human exposure to emissions of various pollutants (such as carbon monoxide (CO), hydrocarbons (HC), particulate matter (PM), nitrogen oxides (NO_x), sulfur dioxide (SO_2) and volatile organic compounds (VOCs)) from traffic, power plants, and diesel generators increases the risk of respiratory and cardiovascular diseases, neurological disorders, cancer, and fertility problems (Rumana et al., 2014; Calderon-Garciduenas et al., 2008; Nakano and Otsuki, 2013; Deng et al., 2016).

In Lebanon, and especially in Beirut, electricity is generated, during outage hours (i.e. when there is no electricity supplied by state-owned electricity suppliers, such as Electricité du Liban (EDL)), through privately owned diesel generators. Recent surveys (Baayoun et al., 2019; Shihadeh et al., 2012) showed that there is on average one diesel generator per two buildings in Beirut. These generators are usually located on street level, in basements, or on rooftops. In addition to releasing anthropogenic heat, emissions from these generators in Hamra, a dense neighborhood in Beirut, were shown to lead to additional daily exposure to airborne carcinogens such as Particle-bound Polycyclic Aromatic Hydrocarbons (PPAH) by about 65% for an outage period of 3 h (Helou, 2012). Furthermore, heavy traffic in the city is another source of anthropogenic heat and pollution. Given the lax governmental regulations that control pollutant emissions from the car fleet, traffic is a significant contributor to both the UHI and air pollution (Halabi et al., 2018).

In this paper, we propose a novel methodology to find optimum values of key urban parameters relevant to the UHI effect in data-scarce urban environments and to improve temperature forecasts in such regions using the obtained values. The objectives of this work are to (1) assess the UHI effect in Beirut in terms of the associated temperature rise, (2) investigate and quantify the key parameters contributing to this effect, and (3) improve the temperature forecast in Beirut city by taking these parameters into account. This is accomplished by comparing predictions, using the single-layer urban canopy model (UCM) coupled with the Weather Research and Forecasting model (WRF), with measurements. To provide a more accurate representation of Beirut in UCM, the urban morphology needs to be accounted for and the urban parameters need to be calibrated to reflect the urban characteristics of Beirut and to minimize the difference between the measured and the forecasted temperature. This process is particularly important for urban environments where data is scarce, as is the case with Beirut city. As a matter of fact, one study (Waked et al., 2013) conducted in Beirut to model pollution dispersion in the city during the summer, using WRF to get meteorological data, relied on default urban parameters due to the lack of data corresponding to such parameters. Another study (Abdallah et al., 2018) that aimed at assessing air quality modeling over Lebanon, also using WRF as a meteorological driver, did not use UCM at all due to the scarcity of geometrical and thermal data that UCM depends on. This proves the need for obtaining such urban parameters for Beirut city.

This paper is organized as follows: Section 2 discusses the methodology used in this work in terms of the modeling tool, domain setup, initial and boundary conditions, tuning process, observational data, and model evaluation. Section 3 highlights optimum values that resulted from the tuning process using statistical analysis, compares temperature predictions – using the tuned parameters – with observations, provides a validation of the obtained values based on physical arguments and concludes with some metrics of urban complexity that contribute to the UHI effect in Beirut. Finally, section 4 provides a summary and sheds the light on some future work.

2. Methodology

2.1. The modeling tool

In this study, the Weather Research and Forecasting model (Skamarock et al., 2008) (WRF, version 3.9) was used. WRF is a nonhydrostatic, compressible model that uses a mass coordinate system with a terrain following coordinates. It is the next generation open-source mesoscale numerical weather prediction tool designed for both atmospheric research and operational forecasting applications and can produce simulations based on actual atmospheric conditions or idealized conditions with high accuracy (Ching, 2013; Tewari et al., 2006). Additionally, it has a myriad of options for physical processes, land surface models, cumulus, and planetary boundary layer parameterizations. In terms of the land surface model and microphysics, the unified Noah land-surface model (Tewari et al., 2016) with four soil layers and the WRF single-moment 3-class simple ice scheme (Hong et al., 2004) were used, respectively. Regarding radiation schemes, the Rapid Radiative Transfer Model was chosen for longwave radiation (Mlawer et al., 1997) while the Dudhia scheme (Dudhia, 1989) was selected for parameterizing shortwave radiation. Additionally, cumulus parameterization was turned on for the two outermost domains (see section 2.2) employing the Kain-Fritsch scheme (Kain, 2004). Finally, the Revised MM5 Monin-Obukhov scheme (Jiménez et al., 2012) was utilized for the surface-layer and the YSU scheme for the

planetary boundary layer (Hong et al., 2006).

To parametrize the effects of urbanization on the urban microclimate, different urban canopy models were developed. These are (1) the bulk urban parametrization which represents zero order effects of urban surfaces (Liu et al., 2006) with the following parameters embedded within the Noah land surface model: roughness length of 0.8 m to represent drag caused by urban surfaces, surface albedo of 0.15 to reflect shortwave radiation trapping, high volumetric heat capacity of 3.0 J m^{-3} K^{-1} for urban surfaces and high soil thermal conductivity of 3.24 W/m K^{-1} to reflect heat storage in building walls and roads, and reduced vegetation fraction over urban surfaces to reduce evaporation; (2) single-layer urban canopy model (Kusaka et al., 2001; Kusaka and Kimura, 2004a) referred to hereafter as "UCM" which was developed to model the energy and momentum exchange between urban surfaces and the atmosphere more accurately than the bulk parameterization via incorporation of more realistic representations of these surface geometries. Additionally, it accounts for the 2D nature of street canyons, shadowing from buildings and radiation trapping. One of its distinguishing features is that it accounts for anthropogenic heating (*AH*) through a parameter that is explicitly defined by the user and that has been proven to be a salient parameter (Kusaka and Kimura, 2004b; Sharma et al., 2016); (3) the multi-layer urban canopy model (Martilli et al., 2002) (also called BEP for Building Effect Parametrization) accounts for solar reflection and radiation trapping between buildings. Moreover, it recognizes the fact that buildings vertically distribute heat, momentum, and moisture through the whole urban canopy. However, unlike the UCM where buildings are embedded within the model's first vertical layer, those in BEP extend beyond the first level (Chen et al., 2011). Furthermore, BEP acknowledges the 3D nature of buildings and does not allow for an explicit specification of *AH* but accounts for it implicitly. A major drawback of this sophisticated model is that it requires high vertical resolution in the vicinity of the ground which is only attainable when computational resources are not a constraint (Kusaka and Kimura, 2004b; Chen et al., 2011). To account for the energy exchange between the interior of buildings and the outdoor environment, the building energy model (BEM) was developed by Salamanca and Martilli (2009) (Salamanca and Martilli, 2009) and linked to BEP. Although the coupled BEP + BEM represents energy exchange between urban structures and the environment more accurately, it is computationally expensive and involves a number of parameters relevant to the heating/cooling equipment for which data is not available. Therefore, as a compromise between the bulk urban parametrization and the computationally expensive BEP and BEP + BEM, the UCM was used in this work.

2.2. Domain setup

For this study, a parent domain (denoted by D1) and two nested domains (denoted by D2 and D3 respectively) were used. As can be seen in Fig. 1, the largest domain D1 constitutes a part of the eastern Mediterranean region while the nested domains D2 and D3 represent Lebanon and Beirut, respectively. Domains D1, D2, and D3 are discretized into 100 × 100, 61 × 73, and 40 × 40 grid points in the west-east and south-north directions, respectively. The corresponding respective spatial resolutions in the x and y direction are 9 km, 3 km, and 1 km. In the z direction, we used 30 vertical layers that stretch vertically from the ground to the height at which the pressure is set to 5000 hPa.

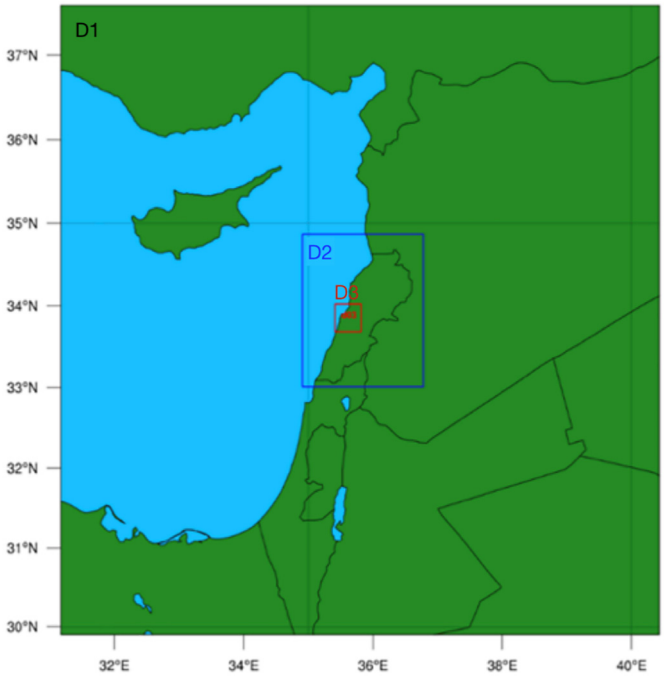

Fig. 1. Domains used in WRF: D1 represents part of the Middle East, D2 represents Lebanon (blue), and D3 represents Beirut (red). (For interpretation of the references to color in this figure legend, the reader is referred to the web version of this article.)

Table 1
UCM physical and geometrical parameters calculated/tuned for Beirut.

Parameter	Calculated/Tuned	Calculated Value	Default Value
Roof albedo	tuned	–	0.2
Wall albedo	tuned	–	0.2
AH (anthropogenic heat)	tuned	–	50 W/m^2
Roof thermal conductivity	tuned	–	0.67 W/m.K
Wall thermal conductivity	calculated	0.997 W/m·K	0.67 W/m·K
Roof height	calculated	19 m	7.5 m
Std dev of roof height	calculated	12.9 m	3 m

For land use, which is essential to urban modeling, we used the dataset from the Moderate Resolution Imaging SpectroRadiometer (MODIS) International Geosphere Biosphere Programme (IGBP), with a spatial resolution of 15 arc-seconds ($\sim$ 450 m).

2.3. Initial and boundary conditions

GFS (Global Forecast System) data (NCEP GFS 0.25, 2015) with a 0.25 degrees resolution from NCEP (the National Centers for Environmental Prediction) was used for the initial and boundary conditions for the WRF-UCM forecasts and hindcasts.

2.4. UCM calibrated/calculated parameters

The urban parameters used in UCM can be broadly divided into two categories: physical, and geometrical (Tewari et al., 2007). Table 1 lists key physical and geometrical parameters and indicates whether each parameter was calculated or tuned for Beirut.

Beirut is considered a high intensity residential area, i.e. a highly populated urban area where vegetation accounts for less than 20% of the land cover while constructed areas account for 80% or more (Tewari et al., 2007). The average buildings' height and its standard deviation were calculated from a shapefile for Beirut which contained the heights of all buildings in the city and which was obtained from the Council for Development and Reconstruction (CDR).

As for the physical parameters, the wall's thermal conductivity was calculated assuming the wall is made up of three layers: a concrete block (10 cm thick) that is sandwiched between two stucco layers (2.5 cm thick each) on both sides. Consequently, the following formula was used:

$$k_{wall} = \frac{l_{total}}{R_{total}} = \frac{2 \times 0.025 + 0.1}{2 \times 0.03519 + 0.08} = 0.997\ \mathrm{W/m{\cdot}K}$$

where l_{total} and R_{total} are the total wall thickness and thermal resistance, respectively.

The remaining physical parameters listed in Table 1 (roof albedo, wall albedo, *AH*, and roof thermal conductivity (k_r)) were tuned, since no representative values exist for Beirut (Waked et al., 2013; Abdallah et al., 2018). The tuning/optimization procedure is discussed in section 2.7.

2.5. Observations

Observations of the temperature and the wind speed from three different stations were used in this study. The three stations, hereafter designated as “Stn1”, “Stn2”, and “Stn3”, are located in *Achrafieh*, *Baabda*, and *AUB* (*The American University of Beirut*), respectively (Fig. 2). The coordinates of these stations are listed in Table 2.

These stations, except for Stn3, are linked with the Weather Underground (November 14, 2018) data repository, which collects data from more than 250,000 weather stations from around the world. This repository, which offers free weather data at different temporal resolutions (daily, weekly, monthly, and yearly), performs perennial quality control checks through algorithms specifically built by data scientists to ensure that the best data is reported. Data from Stn1 and Stn2 was collected from this repository for the whole period of study. Data from Stn3 was directly collected from the weather station on the roof of the *Elmer and Mamdouha Bobst Chemistry Building* at *AUB*.

2.6. Period of study

To obtain statistically meaningful tuned parameters, simulations were performed for 8 days during each of the four seasons. During the summer, fall, winter, and spring seasons of the year 2017, simulations were performed from the 20th (00:00:00 UTC) till the 27th (23:59:59 UTC) of July, October, January, and April, respectively. These choices are based on (i) the requirement that the observed data is representative of the season during which they were measured, and on (ii) the availability of the observed data. Data from Stn3 (see section 2.5) was only available for the months of July and October 2017. In addition, the first 24 h of each simulation were considered as a spin up period and were consequently left out of the analysis. Therefore, simulated data from the 21st to the 27th of each month were used in the statistical analysis.

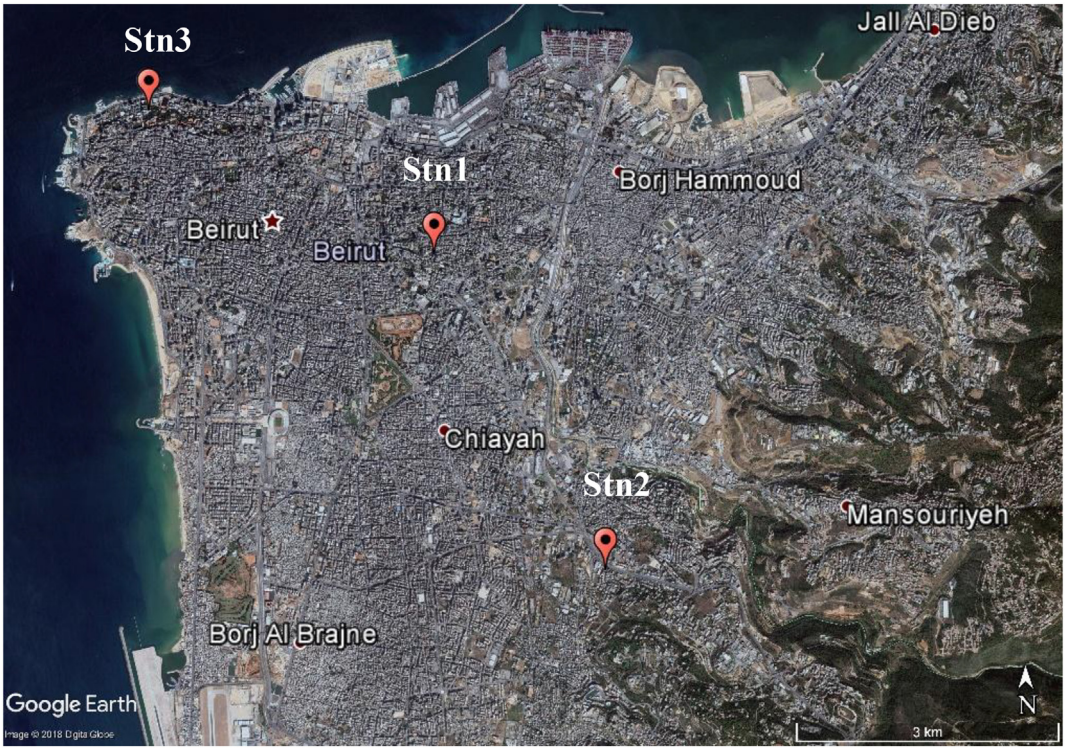

Fig. 2. Locations of the observational stations used are marked on a satellite image for Beirut. Source: Google Earth.

Table 2
Latitude, Longitude, Elevation, and heights above ground level of the three stations.

Station	Lat	Lon	Elevation[a]	Ground level height
Stn1	33.885	35.516	103 m	32 m
Stn2	33.851	35.538	110 m	21 m
Stn3	33.901	35.479	40 m	21 m

[a] Elevation is above sea level.

2.7. The tuning procedure

We point out here that while the roof albedo, wall albedo, and roof thermal conductivity are constant, the anthropogenic heat is time dependent. Values of the roof albedo, wall albedo, and roof thermal conductivity were obtained based on statistical analysis of the simulations performed during the months of July and October in 2017. These values were optimized by minimizing the difference between the observed temperature (*T*) and wind speed (*WS*) and those predicted by WRF-UCM simulations. These optimum values of the roof albedo, wall albedo, and roof thermal conductivity were then used to optimize the value of *AH* using statistical analysis of WRF-UCM simulations for the months of July, October, January and April to get corresponding optimum values for *AH*. Note that these choices were largely constrained by the availability of observations.

A flowchart of the tuning procedure is presented in Fig. 3. The procedure involves carrying out simulations over the ranges of values and increments of the tuned parameters listed in Table 3.

For each value of the selected parameter, the temperature and wind speed were predicted by the WRF-UCM simulation over a 7-day period, on a 1 km grid (representing D3). The predicted values, interpolated onto the locations of the stations, were compared with the observed values at these locations. Comparison was carried out using the following statistical measures: mean, standard deviation (STD), mean bias (MB), root mean square error (RMSE) and correlation coefficient (CC) where the RMSE was the deciding measure in determining optimum values of the tuned parameters.

The objective is to get optimum UCM parameters that yield predicted temperatures and wind speeds as close as possible to observations. This is accomplished by computing the weighted average of the RMSE of the temperature and the wind speed. Since the scales of the temperature and wind speed are different, the RMSE of each is normalized by the corresponding mean, producing the normalized RMSE (NRMSE). The composite NRMSE (WNRMSE) is finally determined as the weighted mean of the NRMSE with the CC's as weights. The value of the tuned parameter that minimizes WNRMSE is chosen to be the optimal value. This optimum value was then used in the table of UCM urban parameters (URBPARM.TBL).

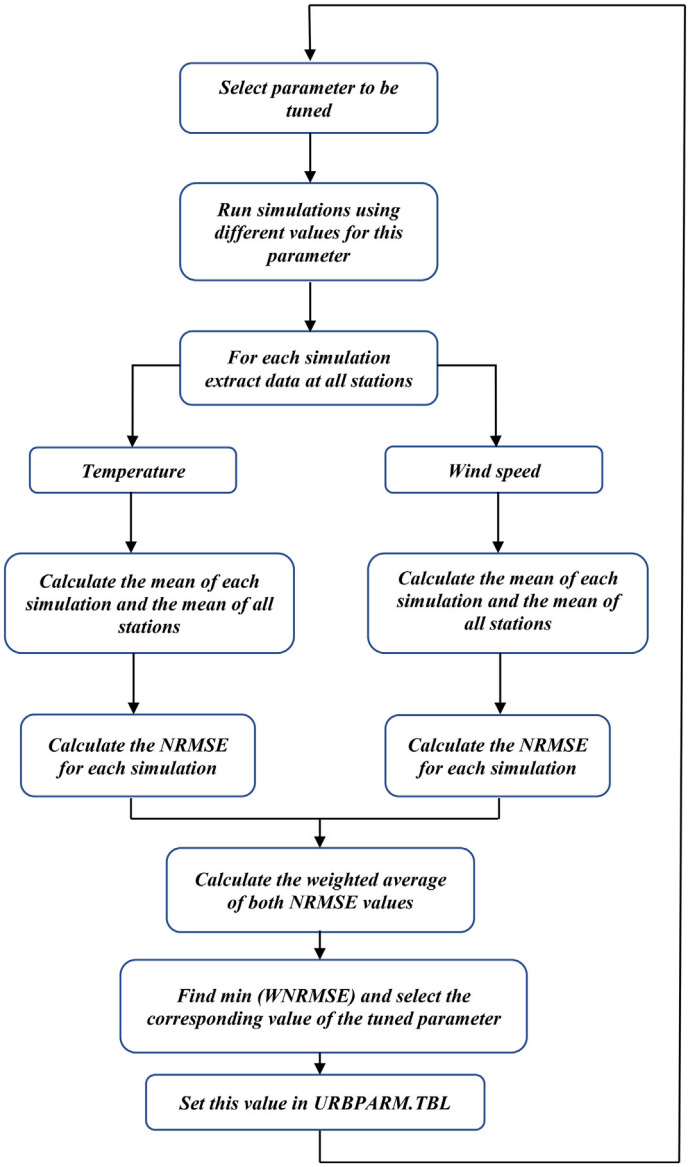

Fig. 3. Flowchart describing the methodology used in the tuning process.

Table 3
Ranges and increments of the parameters used in the tuning procedure.

Parameter	Min	Max	Increment
Roof albedo	0	1	0.01
Wall albedo	0	1	0.01
Roof thermal conductivity (W/m·K)	0	–	0.1
AH (W/m^2)	0	–	10

$$RMSE = \sqrt{\frac{\sum_{i=1}^{n}(P_i - O_i)^2}{n}}\ ,\ NRMSE = \frac{RMSE}{\bar{P}}$$

$$WNRMSE = \frac{NRMSE_T * CC_T + NRMSE_{WS} * CC_{WS}}{CC_T + CC_{WS}}$$

where P_i is the simulated variable at hour i, O_i is the observed variable at hour i, n is the total number of hours, and $\bar{P}$ is the average value of the simulated variable. It is to be noted that since all three stations are situated in the vicinity of the Mediterranean sea, the

Table 4
Optimum values obtained from the tuning process.

Parameter	July	October	January	April	Average
Roof albedo	0.03	0.03	–	–	0.03
Wall albedo	0.06	0.04	–	–	0.05
Roof thermal conductivity	0.4	0.5	–	–	0.45
AH	510	280	610	210	402.5

land-sea breeze circulation affects both measured temperatures and wind speeds, thereby affecting the tuned values.

3. Results and discussion

During July and October, the tuning process showed that the optimum values of the roof and wall albedos, which corresponded to the minimum weighted average of the NRMSE, were below 0.1. Unlike the albedo parameters, obtained values for the roof thermal conductivity were of the same order of magnitude as the default values. Regarding the anthropogenic heat, fine-tuned values ranged between 210 W/m^2 and 610 W/m^2 during the months of July, October, January, and April. Optimum values for the different parameters are summarized in Table 4.

As can be seen in Table 4, the average values of the roof and wall albedos were 0.03 and 0.05, respectively, which are considered low indicating that most of the incoming solar radiation gets absorbed by the different building surfaces. In terms of *AH*, the highest value was in January and the lowest was in April which was expected because in January, the coldest season in Beirut, domestic hot water and heating demands are usually the highest while in April, which is characterized by moderate weather conditions, almost no heating/cooling is required and domestic hot water demands are generally lower than those during the other months considered in the study. Besides that, the optimized value of *AH* was notably high in July primarily due to air conditioning (AC) that is heavily used during this month which is characterized by hot and humid weather conditions. Consequently, all generated heat gets rejected to the urban environment through condensing units.

In what follows, we examine the differences between the following three types of simulations: (i) WRF simulations in which no UCM was used (noUCM), (ii) WRF-UCM simulations using the default UCM parameters (UCMdefault), and (iii) WRF-UCM simulations using the optimized UCM parameters listed in Table 4 (UCMOptimized). Fig. 4 shows plots comparing the average simulated temperatures (averaged over all stations) to observed temperatures (averaged over all stations) during the studied periods. It should be noted that in the legend, the optimum value of *AH* was associated with “UCMOptimized” because this parameter affected simulated variables significantly compared to the other parameters.

As can be clearly noticed, all simulations produced a temperature profile that generally resembles that produced by observations especially during the morning of January 25th in which a temperature peak was observed and during April 23rd in which a noticeable temperature drop occurred. It can also be seen from the figure that UCMOptimized produced a temperature profile that is generally higher than that produced by noUCM and UCMdefault simulations, except for the month of April, where the three types of simulations produced very similar values. Furthermore, during the month of October (Fig. 4(b)), UCMOptimized was generally able to capture the average observed temperatures during most of the days under study.

Table 5 contains a statistical evaluation of the average temperatures shown in Fig. 4 in terms of the Average, Mean Bias, RMSE, and CC. Results show that except for the UCMOptimized simulation during October, a cold bias (negative Mean Bias) was observed for all other simulations with a minimum of 0.02 °C and a maximum of 2.28 °C in absolute value. Furthermore, the statistical analysis confirms that results obtained from the UCMdefault simulations are the least accurate since the absolute value of the Mean Bias and the RMSE were generally the highest during all months, when compared to noUCM and UCMOptimized simulations. Additionally, it can be observed that the UCMOptimized simulation during October produced temperatures with highest accuracy when compared to observations where the Mean Bias, RMSE, and NRMSE values were the lowest (0.02 °C, 1.07 °C, and 0.04, respectively). Also, comparing UCMOptimized simulations for all months showed that the one performed during January produced the highest RMSE (1.93) and NRMSE (0.13) which may be attributed to the fact that observed wind speeds during this month were highly variable due to high wind gusts resulting in simulated wind speeds with high RMSE and NRMSE hence affecting the selection of the optimum value of AH. A closer look at the differences in the average error (Mean Bias) between the three UCM permutations shows that the highest differences occurred in July and January where UCMOptimized improved simulated temperatures by 1.19 °C and 1.34 °C during July and by 1.14 °C and 1.24 °C during January when compared to noUCM and UCMdefault simulations, respectively. A common notable parameter for all simulations during all months is the correlation coefficient which was relatively high during all months reaching a value as high as 0.91 during April.

To further study the difference between simulations in which no UCM was used and those in which UCM was used with optimized parameters during different times of the day, simulated temperatures at 8:00 a.m., 12:00 p.m., and 8:00 p.m. were averaged over all 7 days during October, which is the month that resulted in the highest accuracy as previously discussed, and color maps were produced (Fig. 5). The first column represents noUCM temperature contours, the second column represents contours produced by UCMOptimized and the third column represents the difference between UCMOptimized and noUCM temperature values (UCMOptimized minus noUCM). As can be seen in Fig. 5, a significant difference in temperature between noUCM and UCMOptimized simulations exists at 8:00 a.m. and 8:00 p.m. while there is no noticeable change at noon indicating that both simulations produced

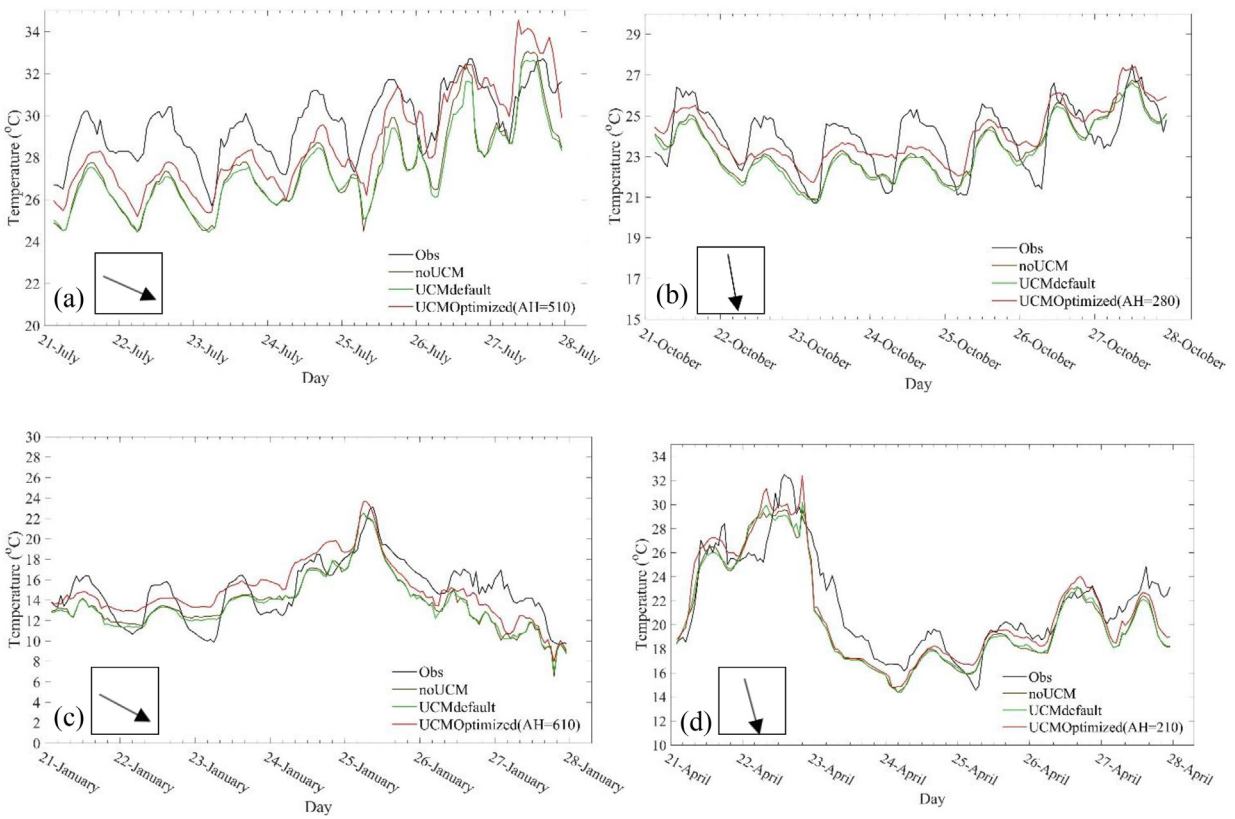

Fig. 4. Comparison between average observed (obs) and simulated temperatures with different permutations of UCM during (a) July (b) October (c) January and (d) April in the year 2017. The insets represent synoptic wind directions averaged over the whole study period where the north is along the positive y-axis. Temperature profiles were obtained from simulations with 1 km resolution and the mean synoptic wind was obtained from the domain with 9 km resolution.

Table 5
Statistical parameters for the average temperatures during July, October, January and April in the year 2017.

		Average	Mean Bias	RMSE	NRMSE	CC
July	Obs	29.63				
	noUCM	27.50	−2.13	2.43	0.09	0.83
	UCMdefault	27.35	−2.28	2.53	0.09	0.82
	UCMOptimized(AH = 510)	28.69	−0.94	1.63	0.06	0.83
October	Obs	24.03				
	noUCM	23.37	−0.66	1.25	0.05	0.74
	UCMdefault	23.25	−0.78	1.31	0.06	0.74
	UCMOptimized(AH = 280)	24.05	0.02	1.07	0.04	0.73
January	Obs	14.93				
	noUCM	13.77	−1.16	2.11	0.15	0.80
	UCMdefault	13.67	−1.26	2.10	0.15	0.82
	UCMOptimized(AH = 610)	14.91	−0.02	1.93	0.13	0.77
April	Obs	21.73				
	noUCM	20.59	−1.14	2.06	0.10	0.91
	UCMdefault	20.58	−1.15	2.09	0.10	0.91
	UCMOptimized(AH = 210)	21.19	−0.53	1.90	0.09	0.91

comparable results at this time. Average temperature differences between both simulations were approximately 2.1 °C and 1.1 °C at 8:00 a.m. and 8:00 p.m., respectively, while that at noon was approximately equal to 0.3 °C. In addition, it is clearly shown that the fine-tuned UCM with optimum parameters is capable of producing the urban heat island effect during early morning and evening unlike the case when UCM is not coupled with WRF. It is noteworthy that a 24 h *AH* profile was used during all simulations in any given season (refer to Figs. S1-S4) with maximums at 8 a.m. and 5 p.m. The profile used in each season is based on the default UCM profile, which is representative of urban environments and has been used in many studies with no available *AH* data (Ma et al., 2017; Wang et al., 2013; Sailor et al., 2015). We note that the default *AH* daily profile, which consists of 24 coefficients (Tewari et al., 2007)

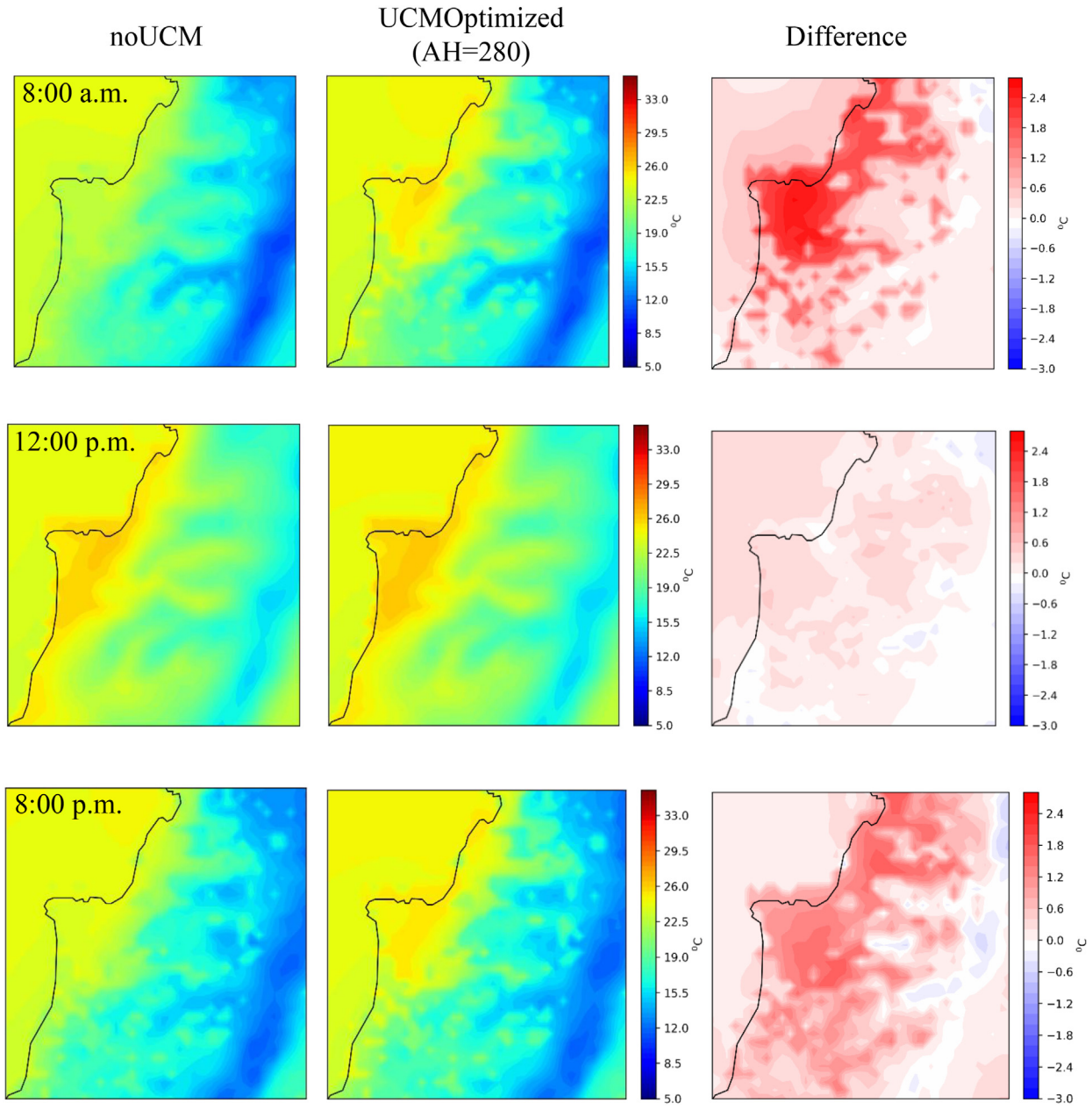

Fig. 5. Color maps showing the temperature distribution over domain D3 for noUCM and UCMOptimized simulations as well as the difference between the two simulations at 8:00 a.m., 12:00 p.m., and 8:00 p.m. during October 2017.

that vary between zero and unity (one coefficient for each hour of the day), gets scaled by the value of *AH* specified by the user (values in Table 4) resulting in *AH* profiles with different magnitudes in each season considered in the study. Although the resultant profiles had seasonal variations as per the values in Table 4, day to day values were held constant in any given season. Bearing this in mind, adopting a different *AH* dirunal profile for every season contributes to the corresponding seasonal diurnal variations of the simulated temperatures (Figs. 4 and 8). To examine the area over which this effect is largely pronounced, the color map corresponding to UCMOptimized at 8:00 a.m. was overlaid on top of a satellite imagery of Beirut (Fig. 6) using QGIS. This showed that the urban heat island effect is primarily located over Borj Hammoud – Dawra areas which are highly dense urban areas with high pollution concentrations especially in Borj Hammoud (Saliba et al., 2010).

As previously mentioned, variations in *AH* affected simulated variables significantly when compared to the remaining tuned parameters. To demonstrate this, the mean temperature, for October 2017, is plotted against *AH*, roof and wall albedos, and the roof thermal conductivity in Fig. 7(a), (b), and (c), respectively. The plots show that a 100 W/m^2 increase in *AH* resulted in a 0.2 °C increase in the average simulated temperature while a 0.05 increase in the roof and wall albedos resulted in a respective 0.011 °C and

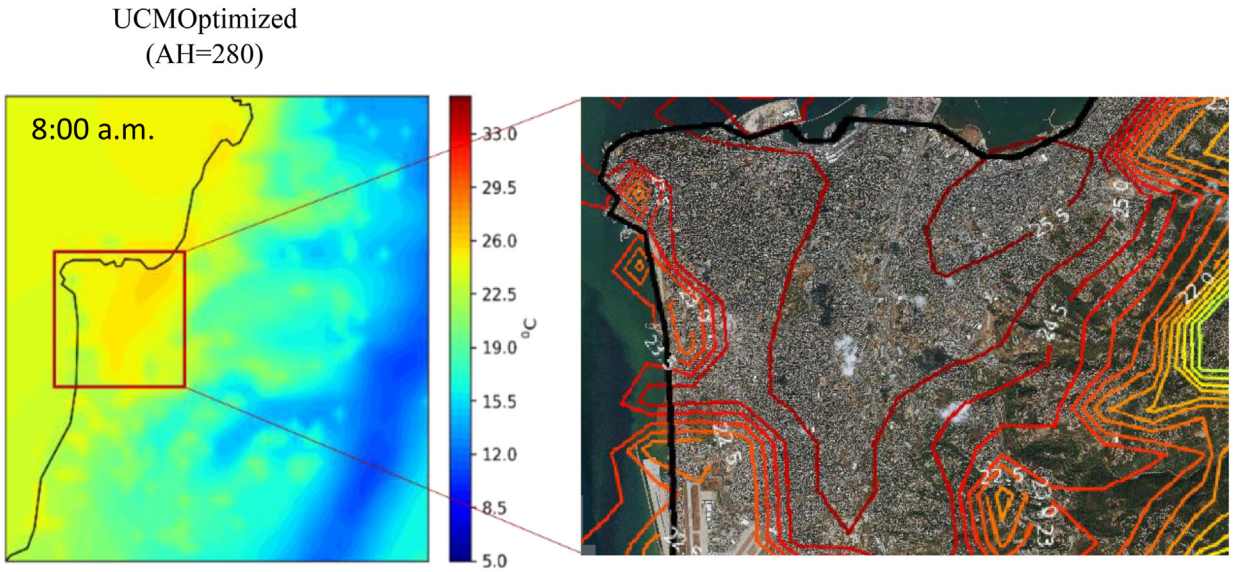

Fig. 6. Color map corresponding to UCMOptimized at 8:00 a.m. overlaid on top of a satellite image for Beirut. Numbers on contour lines are in degrees Celsius.

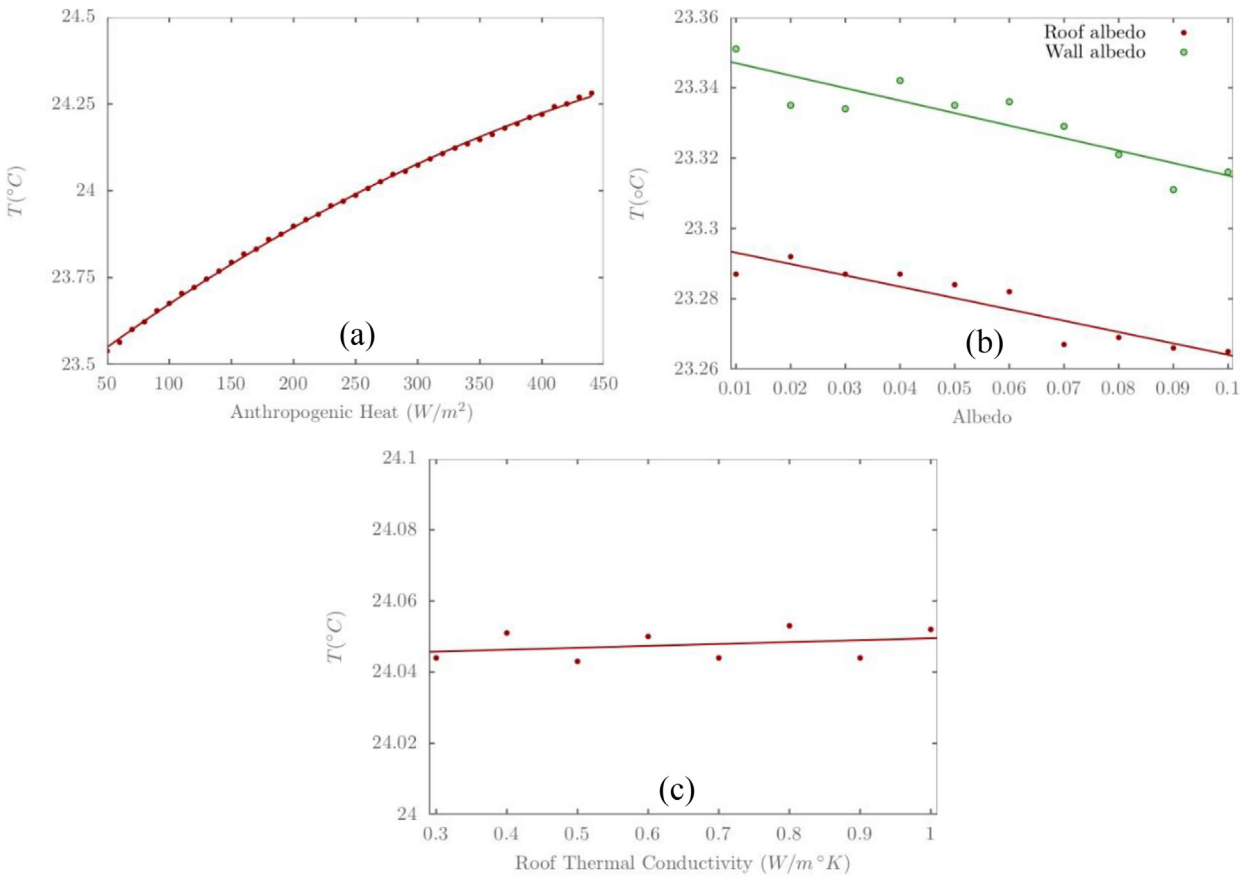

Fig. 7. Variation of the average simulated temperature as a function of (a) AH, (b) roof and wall albedos, and (c) roof thermal conductivity in October 2017.

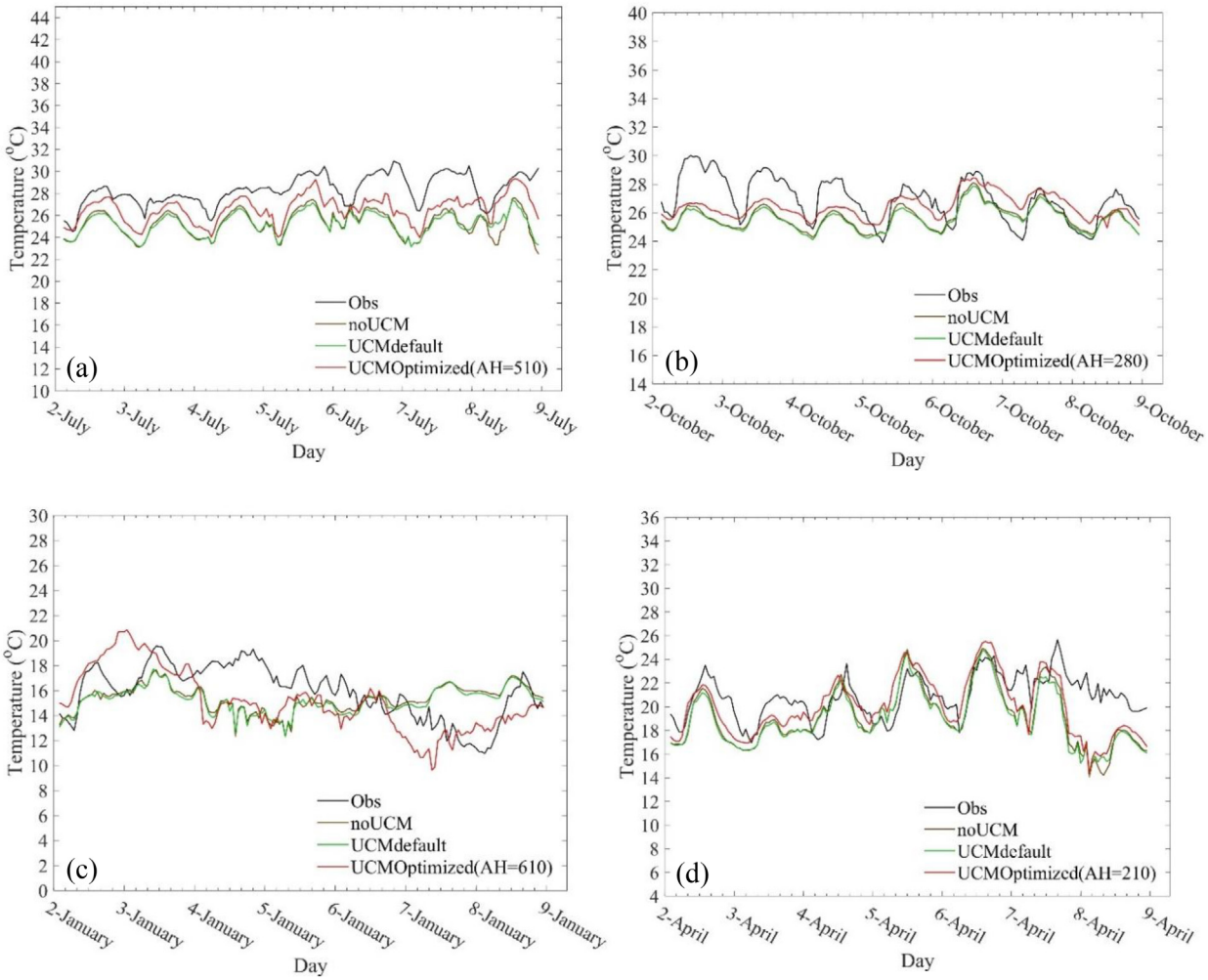

Fig. 8. Comparison between average observed (obs) and predicted temperatures with different permutations of UCM during (a) July (b) October (c) January and (d) April in the year 2018.

0.016 °C decrease in the average simulated temperature. As can be inferred from Fig. 7(c), the impact of changing the roof thermal conductivity on the mean temperature is negligible.

3.1. Predictive UCM

To ensure that the optimized parameters are representative of Beirut not only during the year in which they were tuned, the same parameters were used to predict the temperature during the same months but in the year 2018. Unlike the year 2017, the period chosen during 2018 was from the 2nd (00:00:00 UTC) till the 8th (23:59:59 UTC) (inclusive) of each month since observed data was not available during the period studied in 2017. Average simulated temperatures at Stn1 and Stn2 were compared with average observed temperatures at the same stations and plotted in Fig. 8 (a – d). As can be seen, it is clear that again UCMOptimized was capable of producing a temperature profile with a trend that is generally similar to the one that resulted from observations. A closer look at Fig. 8 (a) clearly shows how the average predicted temperature profile followed the observed one during July 2018 where troughs and crests of both profiles were almost aligned at the same vertical cross-section. Statistical analysis (Table 6) showed that UCMOptimized for this month resulted in an average error of −1.73 °C, RMSE of 2.05 °C, a NRMSE of 0.08, and a correlation coefficient of 0.64 which was the highest among all other simulations during the other months. During the first 3 days of October, the difference between simulated (UCMOptimized) and observed temperatures was about 1.6 °C while this difference reduced significantly during the remaining 4 days of the study period reaching an average of 0.3 °C. Moreover, statistical parameters for this month were generally minimum compared to those of the other months meaning that simulations during October were of the highest accuracy. Regarding January, although the resemblance of the simulated temperature profile to the observed one is not as strong as that obtained for the other months, which again, is explained by the fact that wind speed was included in the tuning process and January is characterized by high wind speeds with relatively high NRMSE, the RMSE and NRMSE were comparable to those obtained

Table 6
Statistical parameters for the average temperatures during July, October, January and April in the year 2018.

		Average	Mean Bias	RMSE	NRMSE	CC
July	Obs	28.31				
	noUCM	25.24	−3.07	3.34	0.13	0.47
	UCMdefault	25.19	−3.12	3.36	0.13	0.47
	UCMOptimized(AH = 510)	26.58	−1.73	2.05	0.08	0.64
October	Obs	26.93				
	noUCM	25.66	−1.27	1.80	0.07	0.56
	UCMdefault	25.54	−1.39	1.88	0.07	0.57
	UCMOptimized(AH = 280)	26.42	−0.51	1.51	0.06	0.40
January	Obs	15.87				
	noUCM	15.33	−0.54	2.52	0.165	−0.10
	UCMdefault	15.20	−0.67	2.52	0.166	−0.06
	UCMOptimized(AH = 610)	15.08	−0.79	2.42	0.161	0.51
April	Obs	20.83				
	noUCM	19.17	−1.66	2.66	0.14	0.56
	UCMdefault	19.01	−1.82	2.70	0.14	0.55
	UCMOptimized(AH = 210)	20.02	−0.81	2.27	0.11	0.54

in January 2017 especially the NRMSE where a difference of 0.03 was observed between the two years. As for the month of April, it is clearly shown how closely the simulated temperature profile followed the observed one except during the last simulation day where UCMOptimized underestimated the temperature. On average, statistical parameters were also comparable to those obtained in April 2017 where a difference of 0.02 in NRMSE was observed. Similar to the observations made in 2017, UCM simulations that included optimized parameters performed better than those that included UCM with default parameters and those that did not include UCM at all. In terms of the average error and with the exception of January, UCMOptimized resulted in the least MB (in absolute value) with values of −1.73 °C, −0.51 °C, and − 0.81 °C during July, October, and April, respectively. Moreover, the RMSE of UCMOptimized was the lowest compared to other UCM permutations during all months attaining a minimum value in October. Additionally, the NRMSE corresponding to UCMOptimized was the minimum compared to all other simulations during all months with the lowest value of 0.06 observed in October as well. Furthermore, a comparison between noUCM, UCMdefault, and UCMOptimized reveals that the latter produced improved temperature forecasts (i.e. less average error) by an average of 1.37 °C during July, 0.82 °C during October, and 0.93 °C during April when compared with noUCM and UCMdefault.

3.2. Physical assessment of the optimal values of the UCM parameters

Optimal values of the UCM parameters were obtained by minimizing the difference between the simulated and observed variables. To further increase the credibility of the outcome of the tuning process, we present here a physical assessment of these values.

Regarding the roof albedo whose optimum value for Beirut was found to be equal to 0.03, a comparison with a color map of roof albedos in Los Angeles created by the Berkeley Lab Heat Island Group (Berkeley Lab Heat Island Group, 2018) showed very close values to the tuned values where the majority of buildings have roof albedos below 0.15. The exact value for any building can be checked by clicking on it, and the value of the roof albedo was 0.04 for a selected building.

It is noteworthy that in a previous study conducted in Beirut (Kaloustian and Diab, 2015), values of 0.225 and 0.7 were used for the roof albedo and values of 0.275 and 0.7 were used for the wall albedo which are higher than the values obtained by optimization mainly because values obtained in this work represent “effective” albedos meaning that the values obtained take into account the effect of surrounding objects. For example, the roof albedo obtained represents the combined effect of the roof material and everything on the roof such as water tanks, the piping system, satellite dishes and solar water heaters which are usually placed on the roofs in Lebanon.

Concerning the roof thermal conductivity, a lower bound was calculated using the Thermal Standard for Buildings in Lebanon (Order of Engineers and Architects of Beirut and LIBNOR, 2010) which was published in 2010 by different entities including the Order of Engineers and Architects of Beirut. This standard includes the maximum allowable overall heat transfer coefficient (U-value) for the roof and the corresponding reciprocal of the convection heat transfer coefficients inside ($1/h_i$) and outside ($1/h_o$) the building. By using the relation between the U-value, the thermal resistance, and the thermal conductivity, the roof thermal conductivity was found to be equal to 0.23 W/m·K by assuming that the roof is made up of a slab that is 30 cm thick. However, most of the buildings in Beirut were built before 2010 which means that they were less resistant and consequently, they had a higher thermal conductivity; hence the average value obtained by optimization (0.45 W/m·K) was acceptable.

$$U_{roof} = \frac{1}{R_i + R_r + R_o} = \frac{1}{\frac{1}{h_i} + R_r + \frac{1}{h_o}}$$

$$\Longrightarrow 0.71 = \frac{1}{0.09 + R_r + 0.05} \Longrightarrow R_r = 1.26\ \mathrm{m^2 \cdot K/W}$$

Table 7
Calculating a rough estimate of Q_{noDG} generated in Beirut.

Total (TJ/year)	265,289
Q_L (W)	16,824,527,316
Q_B (W)	2,726,213,568
Q_{noDG} (W/m^2)	152

$$but\ R_r = \frac{l_r}{k_r} \Longrightarrow k_r = \frac{l_r}{R_r} = \frac{0.3}{1.26} = 0.23$$

$$\Longrightarrow k_r = 0.23\ \mathrm{W/m{\cdot}K}$$

Although the wall thermal conductivity was not found by optimization, the validity of the calculated value was checked in a similar fashion to the roof thermal conductivity where the maximum allowable U-value for the wall is 1.6 W/m·K (assuming that the majority of buildings in Beirut are residential). By using the wall's configuration previously mentioned, the maximum allowable thermal conductivity, per the standard, is equal to 0.33 W/m·K. Again, since most of the buildings in the city were built long before the standard was created meaning that they were less resistant, the calculated value was acceptable.

As for the anthropogenic heat, Lebanese fuel imports during the year 2016 (7,803,792 metric ton), which were obtained through private communication with the Ministry of Environment (MoE), were used to get a rough estimate of the equivalent anthropogenic heat generated in Beirut when this amount of fuel is burnt. The data obtained contained the different fuel derivatives imported as well as their corresponding amounts. Fuel imports were classified into two categories the first of which represents the amount of fuel used by diesel generators and the second represents the amount of fuel used for all other purposes (such as the mobile sector, space heating and cooling, and cooking to name a few).

To calculate the heat generated by burning these amounts of fuel, the calorific value (CV) of all these fuel derivatives were obtained from a report published by MoE (Ministry of Environment, 2015). Having obtained the CV for each fuel type, it was then multiplied by the corresponding mass of the fuel to get the heat generated by burning the given amount of this fuel type. To get the value of *AH* which is represented in W/m^2 and which is generated by burning fuel that is not used by diesel generators, the resulting total energy of 265,289 TJ/year (Table 7) was converted to J/s (W) assuming that heat is released for 12 h per day. This calculated value (Q_L), however, represents *AH* released in the whole country. Hence, to get the fraction of this heat that is generated in Beirut only, the average annual consumption per capita in Lebanon (United Nations Development Programme (UNDP), 2007) (Table 8) was used assuming that the numbers obtained reflect to some extent the relative fuel consumption in each governorate. Consequently, to estimate the amount of *AH* generated in Beirut only (Q_B), the weighted-average of Q_L was calculated using the ratio for Beirut as a weight. Finally, Q_B was divided by the area of Beirut to get the amount of heat generated in Beirut per meter square (Q_{noDG}) which is representative of the average *AH* generated in the city, again, due to burning fuel that is not used by diesel generators. This value was estimated to be equal to 152 W/m^2. On the other hand, to estimate the amount of *AH* resulting from fuel utilized by diesel generator sets (Q_{DG}), fuel amounts used for such purpose in Beirut city were estimated using a bottom-up and a top-down approaches. In the bottom-up approach, fuel consumption of diesel generators in a neighborhood of Beirut was estimated based on a survey and then fuel consumption in the city was found by extrapolation. In the top-down approach, the amount of fuel consumed by diesel generators in the city was calculated from national fuel imports data based on some scaling factors (Baayoun et al., 2019). The former approach resulted in 879 MT/3 h/day and the latter resulted in 615 MT/3 h/day. These numbers were used to calculate an upper bound and a lower bound for *AH* generated in the city. Again, by using the appropriate CV for each fuel type utilized by diesel generators, the bottom-up approach resulted in 196 W/m^2 and the top-down approach resulted in 137 W/m^2. By adding Q_{noDG} and Q_{DG}, we obtained a range for the total *AH* released in the city (Q_t) with a minimum of 289 W/m^2 and a maximum of 348 W/m^2. Table 9 summarizes these calculations.

As can be seen, the estimated range of *AH* is close to the average value obtained by the tuning process (402.5 W/m^2). The difference, however, could be attributed to other scaling factors (not only the amount of expenditure and population) that affect energy consumption in urban versus rural areas. For instance, industrial and commercial activities (UN-Habitat, n.d.), the level of income (Chun-sheng et al., 2012), the amount of energy demanding appliances and facilities in addition to energy tariffs (Bekhet and

Table 8
Average annual consumption per capita (in 1000 LBP) in 2004–2005 in the different governorates. Source: (United Nations Development Programme (UNDP), 2007).

Average Annual Consumption Per Capita (in 1000 LBP)		Population	Total Annual Consumption	Ratio[a]
Beirut	6514	390,503	2,543,736,542	1.00
Mount Lebanon	4512	1,501,570	6,775,083,840	2.66
Nabatieh	3924	768,709	3,016,414,116	1.19
Bekaa	3385	471,209	1,595,042,465	0.63
South	3007	401,197	1,206,399,379	0.47
North	2532	221,846	561,714,072	0.22

[a] The ratio is the value of the total annual consumption corresponding to any governorate divided by that of Beirut.

Table 9
Calculated range of the average AH released in Beirut city.

	Top-Down Approach	Bottom-Up Approach
Q_{DG} (W/m^2)	137	196
Q_t (W/m^2)	289	348

bt Othman, 2011) are some other factors by which energy consumption in urban and rural areas is affected. Note also that the numbers used in the calculations represent only imported amounts of fuel that are recorded. If numbers corresponding to fuel reserves and fuel that is imported through illegal means were available, the calculated values would undoubtedly be higher and consequently, a closer match would be expected.

To provide further assessment of the tuned parameters, a comparison was performed with the Urban Canopy Parameters (UCPs) corresponding to the Local Climate Zone (LCZ) classification map created for Beirut city (Kaloustian and Bechtel, 2016) using the World Urban Database and Access Portal Tool (WUDAPT) (Stewart and Oke, 2012). Based on that study (Kaloustian and Bechtel, 2016), Beirut was considered a mixture of zones LCZ1 and LCZ2 which correspond to "Compact High-Rise" and "Compact Mid-Rise" zonal classifications, respectively. By referring to the physical properties associated with such zones, one can see that the surface albedo corresponding to both LCZ1 and LCZ2 is in the range of 0.1–0.2 which is not very far the average value of both the wall and roof albedos obtained in this work which is equal to 0.04. This mismatch is not surprising since, again, the albedo obtained in this work represents what we referred to as the effective albedo. Additionally, the mean annual anthropogenic heat associated with LCZ1 is in the 50–300 W/m^2 range and that associated with LCZ2 is less than 75 W/m^2, with the latter being much less than the mean annual obtained in this work (402.5 W/m^2). It is interesting to note, however, that the mean annual *AH* presented in this work falls in the range associated with LCZ10 ($AH > 300$ W/m^2) which characterizes an area with heavy industry suggesting that the amount of *AH* produced in Beirut is of the order of that produced in industrial zones. Although this cross-checking was performed to compare most of the optimized urban parameters with those stemming from the LCZ approach, no definitive conclusions can be made due to (a) the uncertainty in our approach due the lack of enough observational data and (b) uncertainties inherent in the LCZ approach where for example, values of the mean annual *AH* corresponding to the different zones are highly dependent on the latitude, season, and population density of the area of interest (Stewart and Oke, 2012) not to mention uncertainties relating to data precision (Mills et al., 2015; Hammerberg et al., 2018).

3.3. Metrics of urban complexity

We characterized the spatial properties of our study area starting with buildings' orientations. For that we circumscribed the buildings' polygons with ellipses and defined their orientations to be along the angles that ellipses' major axes make with East. Their

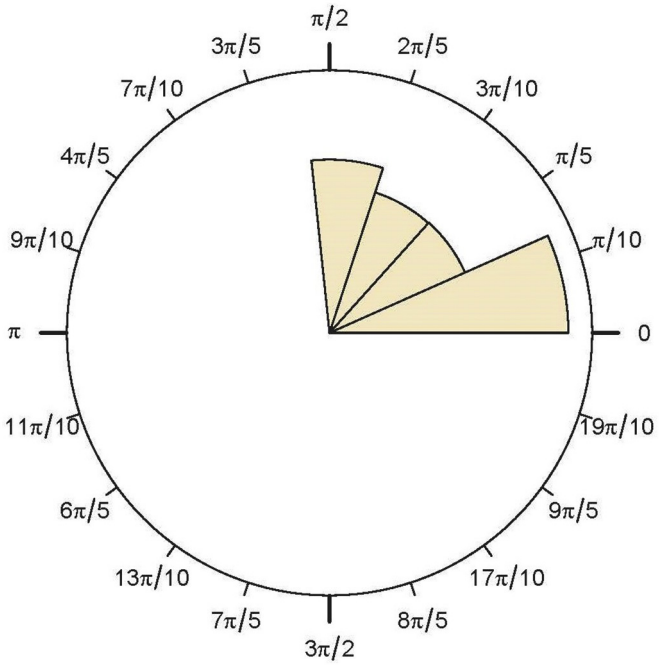

Fig. 9. Buildings' major axes orientations with respect to East-West. The buildings' orientation rose diagram is shown with 0 denoting East-West.

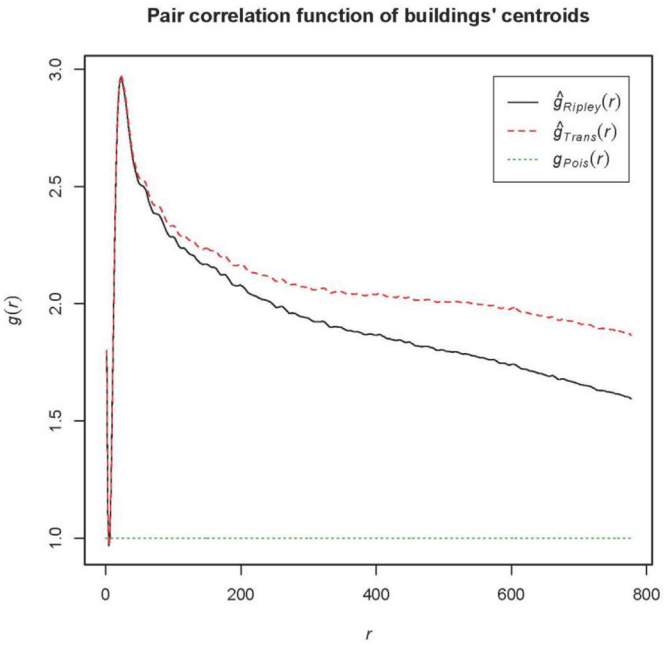

Fig. 10. The pair correlation function of the buildings shown in red is compared to that corresponding to a Poisson process shown in the dashed green line. (For interpretation of the references to color in this figure legend, the reader is referred to the web version of this article.)

distribution is shown in Fig. 9. We note that the majority of the buildings' orientations vary between 0 and pi/10 along East (Mohajeri et al., 2016).

It is shown that east-west orientated urban canyons lead to a small roof-canyon air temperature difference (less than 0.5 °C) (Nakamura and Oke, 1967). Furthermore, shading effects of walls in summer is more favorable in *E*-W oriented streets, whereas in winter, NE-SW or NW-SE oriented streets provide more solar access as opposed to N-S orientation. However, the NE-SW orientation favors morning solar exposure while NW-SE orientation increases the afternoon walls exposure, which could lead to overheating (Shishegar, 2013).

Moreover, we looked at the pair correlation function *g(r)* (Fig. 10), which has been recently used as a metric of urban texture (Sobstyl et al., 2018). More precisely, a building's centroid is considered a point source and the number of buildings falling within a narrow band between r and $r + dr$ is computed. The process is iterated over all points and distances r to compute g, which is then the radial density of the process. We note that g exhibits multiple small peaks which is a characteristic of "liquid structure", that is, the spatial organization of the buildings in the study area does not follow a crystalline order, but rather it is spatially disorganized. The analogy drawn here between the buildings' arrangement in space and that of the atoms in a liquid is indicative of spatial disorder compared to a city whose buildings follow a very well defined spatial planning, which is commensurate to the arrangement of atoms in a solid, or a crystal.

Our aim here was to identity the morphology and geometry of our study area to reveal their connection to UHI. It has been shown in (Sobstyl et al., 2018) that crystalline-like cities, which follow a modular grid-like layout, are more likely to retain heat than their liquid-like disorganized counterparts. We concluded that our study area is rather in the latter category. Therefore, in our case counter effects to this liquid-like urban texture are at play which are associated with the city's dominant buildings' materials, like concrete which insulates more heat, and potentially their heights distribution and density, which we will explore in the below sections.

Additional urban geometry descriptors contribute to the urban microclimate. Density, which is defined to be the ratio of the total built area to the city area is one important indicator. Increasing the building density could lead to trapping of radiation caused by numerous reflections within the canyon. In addition, the long-wave radiation is more likely to be confined due to the limited visible fraction. Moreover, the denser the environment is the more it contributes to wind flow blocking within the canopy layer.

Converse effects have also been reported whereby high density contributed to lower air temperature mainly due to high-rise buildings which reduce the direct solar radiation by providing more shading, thus increasing mutual solar absorption leading to a reduced albedo (Lin et al., 2017). Therefore, we investigated the vertical dimension of our study area and followed the distribution of the buildings' heights from sea level, which is shown in Fig. 11. In our study area, the total area of buildings sums up to 4,900,975 m^2 compared to the study area's 18,000,000 m^2 for which the density is 0.27.

The buildings' heights are known to affect the urban albedo, which is high in both high- and low-density urban forms, since in the former it is largely controlled by the radiation reflected off of the rooftops while in the latter it is controlled by that of the road surface, whereas medium-density configurations exhibit the lowest albedo. Moreover, non-homogenous roof heights are known to create rougher surfaces that lead to higher absorption of solar radiation (Lin et al., 2017; Erell et al., 2012), which is the case in our study area. Both the medium-density and heights' distribution in our study area lead to a low albedo.

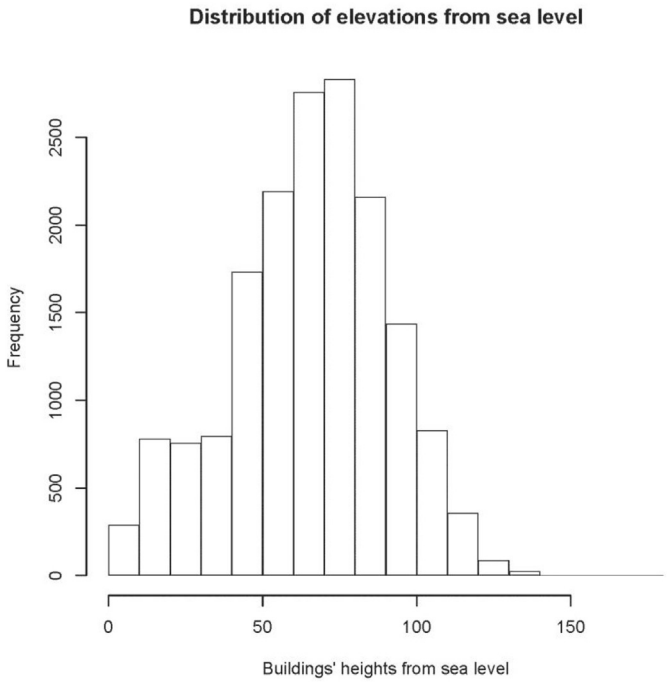

Fig. 11. Buildings' heights distribution.

It is noteworthy that additional urban metrics such as the streets' aspect ratio together with the streets' orientation, which are deemed vital, can be studied. However, given the lack of the street width data for Beirut city, such analysis was not possible.

3.4. Uncertainty quantification

Although a physical assessment of the tuned parameters was performed as previously shown and some urban metrics were analyzed to evaluate the validity of the optimized parameters, uncertainties in the proposed tuning methodology exist as is the case with any model-based fitting approach. As such, uncertainties in the proposed novel method arise from uncertainties in the WRF model, the UCM model, and the observational stations. While uncertainties in WRF and UCM are generously discussed in the literature (Crétat et al., 2012; Yang et al., 2012; Angevine et al., 2014; Wang et al., 2011), major uncertainties in the observational data used in this study are yet to be addressed. First, considering only three stations for the tuning process is a major uncertainty which can be reduced had more stations with equally reliable data become available. Second, uncertainties also arise due to the siting of the measuring stations; for example, Stn3 reflects urban effects to a lesser degree than Stn1 and Stn2 given that, in reality, Stn3 is surrounded by some green areas while the model considers the cell in which it resides in as urban. Finally, another possible source of uncertainty is synoptic and mesoscale effects such as land and sea breeze circulations (see Fig. 4) which could have affected measurements during the periods considered for the tuning process.

4. Conclusion

This paper presented a novel approach to find optimal values of key urban parameters relevant to the UHI effect in urban environments that are characterized by data scarcity. Consequently, obtained numbers were used to improve temperature forecasts. Optimum values of different physical parameters characterizing the urban environment in Beirut were determined by performing numerous simulations using the numerical weather forecasting tool WRF – coupled with the urban canopy model UCM – and comparing simulated temperatures and wind speeds against observations at different stations that are distributed across the city. Results showed that the effective roof and wall albedos in the city were very low indicating that most of the incoming solar radiation gets absorbed by the different building surfaces. As for the anthropogenic heat, the highest value was found in January (610 W/m^2) which is the month during which domestic hot water and space heating demands are usually at their peaks while the lowest was found in April (210 W/m^2) in which no heating or cooling is required due to moderate weather conditions in this month. The improvement in temperature forecasts resulting from using optimum values was also studied where an improvement by more than 1.1 °C was observed in July when compared to using UCM with default parameters and to not using UCM at all. Although optimum values of the tuned parameters were found by comparing simulated variables with observed ones, additional checks were performed when possible to assess the validity of the obtained values. It is to be noted that the tuned parameters presented in this study were specifically chosen because they can be easily enforced by policy makers at least through the building and construction standards set

by the Order of Engineers and Architects in Lebanon in an attempt to reduce the UHI in the city.

To assess the impact of some urban metrics on the urban microclimate, three different metrics, namely the buildings' orientation, their density and their heights were studied. It was concluded that the spatially disorganized order of buildings in the city as well their medium density and height distribution contribute to the UHI effect. A fourth essential urban metric represented by the aspect ratio of the streets along with their orientation could not be studied due to the lack of data pertinent to street widths.

It is expected that this study will be utilized to mitigate the UHI effect by reducing ambient temperatures in regions where the UHI is most pronounced. Based on the findings of this study, *AH* is the major factor affecting the ambient temperature. In comparison, temperature variation due to changes in the roof albedo, wall albedo and the roof thermal conductivity is relatively insignificant. Consequently, finding ways to reduce the anthropogenic heat released (such as relying more on renewable energy and increasing efficiencies of heat-generating equipment) is expected to result in higher reductions in ambient temperatures than increasing the roof and wall albedos or decreasing the roof thermal conductivity.

Moreover, accurate representation of the UHI enables further investigation of the impact of the UHI on pollution transport. Higher ambient temperatures and surface temperatures are expected to increase the buoyancy of plumes. As a future work, sensitivity analysis could be performed on the tuned parameters to study their relative impact on the urban heat island effect in the city. Moreover, the impact of the land-sea breeze circulation on the optimized values could be investigated by applying the same methodology on an inland urban city which would result in a more generalized approach that can be applied to coastal as well as non-coastal areas. Additionally, pollution dispersion simulations can be performed using the chemistry version of WRF (WRF-Chem) and the parameters already found by optimization to study pollution hotspots in the city and their correlation with the urban heat island effect. Furthermore, other parameters that are believed to affect the horizontal and vertical motions of the flow field and consequently pollution dispersion require further investigation and tuning. Some of these parameters are the roughness length of momentum above buildings, the lower boundary condition for the roof and wall temperatures, as well as the planetary boundary layer scheme. This would result in recommendations for urban planners and lawmakers that would help in developing mitigation strategies.

Funding

This work was funded by the Collaborative Research Stimulus (CRS award #103321) from the American University of Beirut (AUB). The sponsor did not have any involvement at any stage of writing this article.

Acknowledgements

The authors would like to acknowledge Fatima Hussein for providing measurements from the Chemistry Building at AUB.

Declaration of Competing Interests

None.

Appendix A. Supplementary data

Supplementary data to this article can be found online at https://doi.org/10.1016/j.uclim.2020.100648.

References

Abdallah, C., Afif, C., El Masri, N., Öztürk, F., Keleş, M., Sartelet, K., 2018. A first annual assessment of air quality modeling over Lebanon using WRF/Polyphemus. Atmospheric Pollution Research 9 (4), 643–654 2018/07/01/.

AEMS, 2017. The Impact of the Syrian Crisis on the Lebanese Power Sector and Priority Recommendations.

Alberti, M., 2005. The effects of urban patterns on ecosystem function. Int. Reg. Sci. Rev. 28 (2), 168–192.

Angevine, W.M., Brioude, J., McKeen, S., Holloway John, S., 2014. Uncertainty in Lagrangian pollutant transport simulations due to meteorological uncertainty from a mesoscale WRF ensemble. In: (in English), *Geoscientific Model Development,* Vol. 7, No. 6, Pp. 2817–2829, 2014-12-04.

Baayoun, A., et al., 2019. Emission inventory of key sources of air pollution in Lebanon. In: *Atmospheric Environment,* Vol. 215, p. 116871, 2019/10/15/.

Beirut [Online] Available. http://academic.eb.com.ezproxy.aub.edu.lb/levels/collegiate/article/Beirut/109399.

Bekhet, H.A., bt Othman, N.S., 2011. Assessing the Elasticities of electricity consumption for rural and urban areas in Malaysia: a non-linear approach. Int. J. Econ. Financ. 3 (1), 208.

Berkeley Lab Heat Island Group, 2018. (November 29, 2018). Available. https://albedomap.lbl.gov/.

Calderon-Garciduenas, L., et al., Nov 2008. Air pollution, cognitive deficits and brain abnormalities: a pilot study with children and dogs. in eng. Brain Cogn. 68 (2), 117–127.

Chen, F., et al., 2011. The integrated WRF/urban modelling system: development, evaluation, and applications to urban environmental problems. Int. J. Climatol. 31 (2), 273–288.

Ching, J.K.S., 2013. A perspective on urban canopy layer modeling for weather, climate and air quality applications. Urban Clim. 3 (Supplement C), 13–39 2013/05/01/.

Chun-sheng, Z., Shu-wen, N., Xin, Z., 2012. Effects of household energy consumption on environment and its influence factors in rural and urban areas. In: *Energy Procedia,* Vol. 14, Pp. 805–811, 2012/01/01/.

Crétat, J., Pohl, B., Richard, Y., Drobinski, P., 2012. Uncertainties in simulating regional climate of southern Africa: sensitivity to physical parameterizations using WRF. Clim. Dyn. 38 (3–4), 613–634.

Deng, Z., et al., 2016. Association between air pollution and sperm quality: A systematic review and meta-analysis. Environ. Pollut. 208, 663–669 2016/01/01/.

Dudhia, J., 1989. Numerical study of convection observed during the winter monsoon experiment using a Mesoscale two-dimensional model. J. Atmos. Sci. 46 (20),

3077–3107.
Erell, E., Pearlmutter, D., Williamson, T., 2012. Urban Microclimate: Designing the Spaces between Buildings. Routledge.
Halabi, L.E., Helou, J.E., Itani, W., Medlej, S., 2018. Developing Cleaner & Efficient Vehicle Policies in Lebanon.
Hammerberg, K., Brousse, O., Martilli, A., Mahdavi, A., 2018. Implications of employing detailed urban canopy parameters for mesoscale climate modelling: a comparison between WUDAPT and GIS databases over Vienna, Austria. Int. J. Climatol. 38 (S1), e1241–e1257.
Helou, M.A., 2012. Impact of distributed urban generators on household exposure to carcinogenic airborne particles during rolling blackout episodes. In: Masters, Mechanical Engineering, American University of Beirut, AETJ ET:5674:C.1.
Hong, S.-Y., Dudhia, J., Chen, S.-H., 2004. A revised approach to ice microphysical processes for the bulk parameterization of clouds and precipitation. Mon. Weather Rev. 132 (1), 103–120.
Hong, S.-Y., Noh, Y., Dudhia, J., 2006. A new vertical diffusion package with an explicit treatment of entrainment processes. Mon. Weather Rev. 134 (9), 2318–2341.
Jiménez, P.A., Dudhia, J., González-Rouco, J.F., Navarro, J., Montávez, J.P., García-Bustamante, E., 2012. A revised scheme for the WRF surface layer formulation. Mon. Weather Rev. 140 (3), 898–918.
Kain, J.S., 2004. The Kain–Fritsch convective parameterization: an update. J. Appl. Meteorol. 43 (1), 170–181.
Kaloustian, N., Bechtel, B., 2016. Local climatic zoning and urban Heat Island in Beirut. In: *Procedia Engineering,* Vol. 169, Pp. 216–223, 2016/01/01/.
Kaloustian, N., Diab, Y., 2015. Effects of urbanization on the urban heat island in Beirut. In: *Urban Climate,* vol. 14, pp. 154–165, 2015/12/01/.
Kusaka, H., Kimura, F., 2004a. Coupling a single-layer urban canopy model with a simple atmospheric model: impact on urban Heat Island simulation for an idealized case. Journal of the Meteorological Society of Japan. Ser. II 82 (1), 67–80.
Kusaka, H., Kimura, F., 2004b. Thermal effects of urban canyon structure on the nocturnal Heat Island: Numerical experiment using a Mesoscale model coupled with an urban canopy model. J. Appl. Meteorol. 43 (12), 1899–1910 2004/12/01.
Kusaka, H., Kondo, H., Kikegawa, Y., Kimura, F., December 01 2001. A simple single-layer urban canopy model for atmospheric models: comparison with multi-layer and slab models. Boundary-Layer Meteorology, journal article 101 (3), 329–358.
Liang, W., Yang, M., 2019. Urbanization, economic growth and environmental pollution: evidence from China. Sustainable Computing: Informatics and Systems 21, 1–9.
Lin, P., Gou, Z., Lau, S., Qin, H., 2017. The impact of urban design descriptors on outdoor thermal environment: a literature review. Energies 10 (12), 2151.
Liu, Y., Chen, F., Warner, T., Basara, J., 2006. Verification of a Mesoscale data-assimilation and forecasting system for the Oklahoma City area during the joint urban 2003 field project. J. Appl. Meteorol. Climatol. 45 (7), 912–929.
Lu, X., et al., 2019. Analysis of the adverse health effects of PM2.5 from 2001 to 2017 in China and the role of urbanization in aggravating the health burden. Sci. Total Environ. 652, 683–695 2019/02/20.
Ma, S., Pitman, A., Hart, M., Evans, J.P., Haghdadi, N., MacGill, I., 2017. The impact of an urban canopy and anthropogenic heat fluxes on Sydney's climate. Int. J. Climatol. 37 (S1), 255–270.
Martilli, A., Clappier, A., Rotach, M.W., August 01 2002. An urban surface exchange parameterisation for Mesoscale models. Boundary-Layer Meteorology, journal article 104 (2), 261–304.
Mills, Gerald, Ching, L, See, L, Bechtel, B, Foley, M, 2015. Proceedings of the 9th International Conference on Urban Climate. Toulouse, France.
Ministry of Environment, 2015. National Greenhouse Gas Inventory Report and Mitigation Analysis for the Energy Sector in Lebanon.
Mlawer, E.J., Taubman, S.J., Brown, P.D., Iacono, M.J., Clough, S.A., 1997. Radiative transfer for inhomogeneous atmospheres: RRTM, a validated correlated-k model for the longwave. J. Geophys. Res.-Atmos. 102 (D14), 16663–16682.
Mohajeri, N., Upadhyay, G., Gudmundsson, A., Assouline, D., Kämpf, J., Scartezzini, J.-L., 2016. Effects of urban compactness on solar energy potential. Renew. Energy 93, 469–482.
Nakamura, Y., Oke, T.R., 1967. Wind, temperature and stability conditions in an east-west oriented urban canyon. Atmos. Environ. 22 (12), 2691–2700 1988.
Nakano, T., Otsuki, T., Nov 2013. Environmental air pollutants and the risk of cancer]," (in jpn. Gan To Kagaku Ryoho 40 (11), 1441–1445.
NCEP GFS 0.25, 2015. Degree global forecast grids historical archive. In: Boulder, C.O. (Ed.), Research Data Archive at the National Center for Atmospheric Research. Computational and Information Systems Laboratory.
November 14, 2018. Available: www.wunderground.com.
Oke, T.R., 1967. City size and the urban heat island. Atmos. Environ. 7 (8), 769–779 1973/08/01.
Order of Engineers and Architects of Beirut and LIBNOR, 2010. Thermal Standard for Buildings In Lebanon.
ReliefWeb. (2/9/2019) Available. https://reliefweb.int/report/lebanon/lebanon-beirut-mount-lebanon-governorates-profile-october-2018.
Rumana, H.S., Sharma, R.C., Beniwal, V., Sharma, A.K., Jan 9 2014. A retrospective approach to assess human health risks associated with growing air pollution in urbanized area of Thar Desert, western Rajasthan, India. (in eng), J Environ Health Sci Eng 12 (1), 23.
Sailor, D.J., Georgescu, M., Milne, J.M., Hart, M.A., 2015. Development of a national anthropogenic heating database with an extrapolation for international cities. In: *Atmospheric Environment,* Vol. 118, Pp. 7–18, 2015/10/01/.
Salamanca, F., Martilli, A., May 13 2009. A new building energy model coupled with an urban canopy parameterization for urban climate simulations—part II. Validation with one dimension off-line simulations. Theoretical and Applied Climatology, journal article 99 (3), 345.
Saliba, N., El Jam, F., El Tayar, G., Obeid, W., Roumie, M., 2010. Origin and variability of particulate matter (PM10 and PM2. 5) mass concentrations over an eastern Mediterranean city. Atmos. Res. 97 (1–2), 106–114.
Sharma, A., Fernando, H.J.S., Hamlet, A.F., Hellmann, J.J., Barlage, M., Chen, F., 2016. Urban meteorological modeling using WRF: A sensitivity study. In: *International Journal of Climatology,* Vol. 37, No. 4, Pp. 1885–1900, 2017/03/01.
Shihadeh, A., et al., 2012. Effect of Distributed Electric Power Generation on Household Exposure to Airborne Carcinogens: Unintended Consequences of Supply-Side Electric Power Reduction Measures in Poorly Regulated Environments.
Shishegar, N., 2013. Street design and urban microclimate: Analyzing the effects of street Geometryand orientation on airflow and solar access in urban canyons. Journal of Clean Energy Technologies 1 (1).
Skamarock, W.C., et al., 2008. A Description of the Advanced Research WRF Version 3.
Sobstyl, J., Emig, T., Qomi, M.A., Ulm, F.-J., Pellenq, R.-M., 2018. Role of city texture in urban heat islands at nighttime. Phys. Rev. Lett. 120 (10), 108701.
Stewart, I.D., Oke, T.R., 2012. Local climate zones for urban temperature studies. Bull. Am. Meteorol. Soc. 93 (12), 1879–1900.
Tewari, M., Chen, F., Kusaka, H., 2006. Implementation and Evaluation of a Single –Layer Urban Canopy Model in WRF/Noah.
Tewari, M., Chen, F., Kusaka, H., Miao, S., 2007. Coupled WRF/unified Noah/urban-canopy modeling system. In: Ncar WRF Documentation, NCAR, Boulder. 122 November 14, 2018). Available. www.wunderground.com.
Tewari, M., et al., 2016. Implementation and Verification of the United NOAH Land Surface Model in the WRF Model. pp. 11–15.
UN-Habitat Available. https://unhabitat.org/urban-themes/energy/.
UN-Habitat. (2014, 2017) Lebanon – Urban Issues. Available. https://unhabitat.org/lebanon/lebanon-urban-issues/.
UNHCR. (2/2/2019) Available. https://data2.unhcr.org/en/situations/syria/location/71.
United Nations Development Programme (UNDP), 2007. Poverty, Growth & Inequality in Lebanon.
Waked, A., et al., 2013. Modeling air pollution in Lebanon: evaluation at a suburban site in Beirut during summer. Atmos. Chem. Phys. 13 (12), 5873–5886.
Wang, M., Yan, X., Liu, J., Zhang, X., 2013. The contribution of urbanization to recent extreme heat events and a potential mitigation strategy in the Beijing–Tianjin–Hebei metropolitan area. In: *Theoretical and Applied Climatology,* Vol. 114, No. 3, Pp. 407–416, 2013/11/01.
Wang, Z.-H., Bou-Zeid, E., Au, S.K., Smith, J.A., 2011. Analyzing the sensitivity of WRF's single-layer urban canopy model to parameter uncertainty using advanced Monte Carlo simulation. J. Appl. Meteorol. Climatol. 50 (9), 1795–1814.
Yang, B., Qian, Y., Lin, G., Leung, R., Zhang, Y., Fu, Q., 2012. Some issues in uncertainty quantification and parameter tuning: a case study of convective parameterization scheme in the WRF regional climate model. Atmos. Chem. Phys. 12 (5).